

GPU-Accelerated ANNS: Quantized for Speed, Built for Change

Hunter McCoy
Northeastern University
Boston, United States
mccoy.hu@northeastern.edu

Zikun Wang
Northeastern University
Boston, United States
wang.zikun@northeastern.edu

Prashant Pandey
Northeastern University
Boston, United States
p.pandey@northeastern.edu

ABSTRACT

Approximate nearest neighbor search (ANNS) is a core problem in machine learning and information retrieval. GPUs offer a promising path to high-performance ANNS through massive parallelism and co-location with downstream applications, but current GPU indices face three limitations: inability to update without full rebuilds, lack of efficient quantization for high-dimensional vectors, and poor latency hiding due to data-dependent memory accesses.

We present Jasper, a GPU-native ANNS system built on the Vamana graph index that achieves both high query throughput and full updatability via three new techniques: (1) a batch-parallel construction algorithm enabling lock-free streaming insertions, (2) a GPU-efficient RaBitQ implementation that reduces memory footprint up to 8 \times without random access penalties, and (3) an optimized search kernel with improved compute utilization and latency hiding.

Across five datasets, Jasper achieves up to 1.93 \times higher throughput than CAGRA, the current state-of-the-art GPU index, while providing updatability that CAGRA lacks, constructs indices 2.4 \times faster on average, and delivers 19 – 131 \times faster queries than BANG, the previous fastest GPU Vamana implementation.

Artifact Availability:

The source code, data, and/or other artifacts have been made available at <https://github.com/saltsystemslab/JasperGPUANNS>.

1 INTRODUCTION

Nearest neighbor search is a fundamental problem in machine learning and information retrieval. The problem involves finding the k closest points to a query in a high-dimensional space. In this paradigm, complex data such as images, documents, or user profiles are embedded as vectors in a *metric space* (such as Euclidean, Manhattan, Hamming) that enables similarity to be measured through geometric distance. Applications span recommendation systems [28, 31], image retrieval [4, 27], anomaly detection [13, 24, 29], and increasingly, retrieval-augmented generation (RAG) for large language models [26, 37, 38], where relevant context must be retrieved from massive corpora in real time.

Traditional indexing structures such as $k-d$ trees [5] and quad trees [10] provide efficient exact nearest neighbor search in low dimensions, but scale poorly as dimensionality increases. The *curse of dimensionality* [21] causes distances between points to concentrate, with the ratio between nearest and farthest neighbors approaching one. This phenomenon undermines the spatial pruning heuristics that traditional indices rely upon, causing query complexity to degrade toward exhaustive linear scans. Modern embedding models routinely produce vectors with hundreds to thousands of dimensions, limiting the practicality of exact methods.

Approximate nearest neighbor search (ANNS) addresses this challenge by relaxing the exactness constraint. Rather than returning exact nearest neighbors, ANNS returns results within some acceptable error bound. This trade-off enables scalability to high-dimensional datasets. The three dominant paradigms for ANNS are: inverted file indices (IVF) [3, 17, 33, 40], locality-sensitive hashing (LSH) [7, 14, 22], and graph-based indices [8, 9, 12, 15, 18–20, 25].

Graph-based indices achieve the best recall-throughput trade-offs among these paradigms. Recent empirical studies have consistently demonstrated this advantage [15]. Graph-based indices construct a *navigable search graph* [18] where vertices correspond to vectors and edges encode neighborhood relationships. Nearest neighbor queries proceed via greedy traversal also known as *beam search*: starting from a designated entry point, the search iteratively expands the closest unvisited vertex until convergence, maintaining a frontier of the best (top k) candidates encountered.

Modern applications require updatable ANNS indexes. Real-world ANNS applications operate at massive scale and require continuous updates due to evolving datasets. Web-scale retrieval systems index billions of vectors: Facebook’s similarity search infrastructure handles over 200 billion embeddings [9], while Microsoft’s Bing uses DiskANN to search over a billion document vectors [1]. These systems must support both millions of queries per second and continuously index updates as new content arrives [31]. Music streaming, product recommendation, and RAG systems depend on scalable and updatable similarity search [32].

The case for GPU acceleration. GPUs offer massive parallelism that promises to accelerate ANNS to achieve high throughput and low latency. Both index construction and search are well-suited to leverage this parallelism because the core operations (pair-wise distance computations) are independent and can execute concurrently across candidates. As dataset size and vector dimensionality grow, so does the available parallel work that GPUs can exploit.

Furthermore, GPUs are already widely deployed in settings where ANNS is most needed. Modern machine learning infrastructure runs on GPU clusters. Using GPUs for ANNS allows organizations to leverage existing hardware rather than provisioning separate CPU-based retrieval infrastructure. This co-location also reduces data movement: embeddings generated on GPU can be indexed and queried without costly transfers to CPU memory.

Challenges in exploiting GPU parallelism for ANNS. Modern GPUs offer thousands of execution units and memory bandwidth exceeding 2 TB/s [23], yet achieving peak performance for ANNS indexing and queries remains difficult. We identify three key challenges in exploiting the massive GPU parallelism.

1) *ANNS workloads need updatability.* Most current GPU indices require a rebuild from scratch in order to process new updates. However, real-world applications such as anomaly detection [13] and

RAG [26, 37, 38] require the ability to modify the index to incorporate new information in search results.

2) *Greedy graph traversal creates irregular memory access patterns.* Unlike dense matrix operations where access patterns are known ahead of time, graph search follows data-dependent paths that vary per query. When different threads in a warp access non-contiguous memory locations, the GPU must issue multiple memory transactions, wasting memory bandwidth. This problem is made worse by the pointer-chasing nature of graph traversal, where each hop depends on the previous result.

3) *ANNS workloads are memory-bound rather than compute-bound.* Each vector dimension is read once, used for a single multiply-add in the distance computation, then discarded. With no data reuse, performance is limited by how fast data can be fetched from memory rather than how fast arithmetic can be performed. For a 128-dimensional float32 vector, the GPU performs 256 floating-point operations but must load 512 bytes of data, a ratio far below what modern GPUs can sustain at peak compute utilization. In our analysis in Section 6.5, we find that the state-of-the-art ANNS search kernels are very close to the peak memory capacity: to further improve performance, data transfer must be reduced.

Limitations of existing GPU ANNS systems. Existing GPU ANNS systems either lack updatability or suffer from poor performance. CAGRA [25], the current state-of-the-art GPU ANNS system, achieves high query throughput by employing a carefully optimized graph structure derived from NN-Descent. However, CAGRA’s graph construction algorithm is batch-oriented, and the system is not designed for incremental updates. In production settings where data arrives continuously, the inability to update the index without full reconstruction is a critical limitation.

BANG [35] is based on an updatable graph structure but suffers from severe performance penalties as it employs product quantization (PQ) [17]¹ for compressing the vectors. BANG extends the Vamana ANNS index [15]; this index structure enables updates (although BANG currently does not implement index updates). However, its reliance on Product Quantization (PQ) limits peak performance. In Section 5, we discuss in detail the limitations of product quantization on GPUs.

Other GPU ANNS systems face their own constraints. GANNS [34] implements HNSW but struggles with the algorithm’s sequential construction dependencies. SONG [42] and GTS [43] target different index structures (fixed-rank graphs and trees, respectively) with different trade-off profiles. None of these systems simultaneously achieve state-of-the-art query performance, efficient construction, and support for streaming updates.

This paper. We present Jasper, a GPU-native ANNS system that addresses the above challenges to achieve high query throughput while supporting dynamic index updates. We make the following contributions:

- **Batch-parallel GPU construction.** We devise a batch-parallel construction algorithm for GPU execution. Rather than using fine-grained locks that create serialization bottlenecks at high-degree vertices, our approach performs beam searches independently,

¹PQ is a quantization technique that reduces vector size by decomposing the original vector into a Cartesian product of independently quantized low-dimensional subspaces.

accumulates candidate edges, sorts them by target vertex, and applies pruning in parallel without needing synchronization.

- **GPU-efficient quantization.** We present the first GPU implementation of RaBitQ [11], a quantization scheme that compresses vectors through randomized rotation and scalar quantization. Unlike product quantization, RaBitQ distance computation requires sequential memory access and simple arithmetic—no codebook lookups. This enables up to 8× memory reduction for vectors and *improved* throughput for high-dimensional datasets, as reduced memory traffic outweighs the modest computational overhead.
- **Optimized search kernel.** We analyze the beam search kernel and identify that for smaller vectors, block size and occupancy dominate performance. Peak throughput occurs at 32 threads per block with 100% occupancy due to better latency hiding across blocks. Our kernel minimizes shared memory usage to maximize concurrent queries per SM (defined in Section 2.2), achieving 70–80% of peak roofline performance [39] and up to 50% higher FLOPS/s than CAGRA at equivalent accuracy.
- **Optimized memory access patterns.** We introduce a tile-based loading scheme that issues blocked 16-byte loads across the threads in a warp simultaneously. Naive implementations either serialize loads through a single thread or issue element-wise loads across the warp (defined in Section 2.2). Our approach achieves both low latency and high throughput by partitioning vectors into 16-byte chunks that are processed in parallel.
- **Systematic performance analysis.** We conduct a detailed empirical study of GPU ANNS optimization strategies. We characterize the trade-offs between per-query parallelism and memory-level parallelism, finding that optimal block sizes differ significantly across datasets. We perform roofline analysis [39] on the state-of-the-art search kernels and find that modern ANNS kernels are memory bound and execute at close to optimal throughput.

Results. Our evaluation on five standard ANNS benchmarks demonstrates:

- Jasper achieves up to 1.93 × higher query throughput than CAGRA, the state-of-the-art GPU index, while providing updatability that CAGRA lacks.
- Compared to BANG, the previous state-of-the-art GPU Vamana implementation, Jasper delivers 19–131 × higher throughput.
- Jasper achieves peak throughput exceeding 13.1 million queries/sec on the BigANN dataset and over 3 million queries/sec on 1,536-dimensional OpenAI embeddings with RaBitQ quantization.
- Jasper’s has the fastest incremental and batch GPU construction: Jasper has a peak insertion throughput of 674K insertions per second and is 2.4× faster on average than CAGRA for index construction across five datasets.
- Our coalesced vector loading scheme improves memory access performance by up to 14% at low beam widths, with no throughput penalty at high beam widths.

Broader implications for GPU system design. The underlying techniques proposed in our work address fundamental challenges in GPU-accelerated irregular workloads more broadly. Our analysis of the trade-off between per-query parallelism and memory-level parallelism applies to any GPU workload with low arithmetic intensity and data-dependent access patterns, such as graph analytics and database

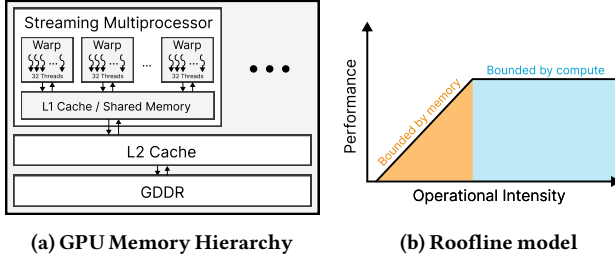


Figure 1: GPU memory hierarchy and roofline model.

query processing. Our roofline analysis confirms that state-of-the-art kernels for irregular workloads already operate near the memory bandwidth ceiling, suggesting that future gains must come primarily from reducing data movement rather than algorithmic improvements alone. These insights provide a template for optimizing other memory-bound, irregular GPU workloads beyond similarity search.

2 PRELIMINARY

This section describes the GPU execution and memory models relevant to building high-throughput ANNS indexes. We first explain the GPU execution model and how work is scheduled on the GPU. We then explain the GPU memory hierarchy and how it affects achieving peak performance. We then examine how these hardware characteristics affect existing GPU ANNS systems and introduce the roofline model [39] as a framework for analyzing their performance.

2.1 GPU execution model

A diagram of the GPU architecture is shown in Figure 1a. A GPU consists of multiple **streaming multiprocessors (SMs)**, each capable of hosting up to 1024 concurrent threads. Tasks on a GPU are executed in a chunk of work called a **kernel**. Each kernel is a single-instruction, multiple-thread (SIMT) function that is executed in parallel by every thread. GPU kernels are executed as collections of *thread blocks* on SMs, each containing up to 1024 threads. Within a block, threads are subdivided into *warps* (groups of 32 threads) that share execution resources and issue memory operations cooperatively. As a result, performance is maximized when threads within a warp follow identical control flow and access contiguous or nearby memory locations. Warps can be further subdivided into *tiles* that divides the resources within a warp for multiple jobs.

ANNS workloads expose fine-grained parallelism during nearest neighbor search as pairwise distances can be computed independently in parallel. Each vector is examined by a *tile*, allowing multiple candidate vectors to be accessed and evaluated in parallel. Tiles are densely packed into warps: larger tiles increase per-probe parallelism by examining more individual vectors faster, while smaller tiles improve latency hiding by enabling additional concurrent memory requests within a warp.

The optimal block and tile configuration depends on the characteristics of the ANNS index, including memory layout, probe fan-out, and candidate filtering costs.

2.2 GPU memory model

The design of concurrent GPU data structures is fundamentally constrained by the underlying memory consistency model, which

governs how memory operations from different threads become visible to one another. In contrast to CPUs that are sequentially consistent, modern GPUs implement a weak memory model based on Relaxed Memory Ordering (RMO) [2]. Under RMO, reads and writes may be freely reordered unless explicitly constrained, and a read in one thread that logically follows a write in program order from a different thread is not guaranteed to observe that write without additional synchronization. GPUs prioritize throughput over latency. With thousands of concurrent threads on GPUs, enforcing strong ordering requires expensive coherence traffic.

Each streaming multiprocessor contains an L1 cache. All threads within an SM share this cache, which is not coherent with L1 caches on other SMs. These per-SM caches connect to a globally coherent L2 cache, which in turn backs the GPU’s main memory (GDDR).

This shared L1 cache is crucial for achieving high performance in GPU applications. A section of this cache can be designated as **shared memory**. Unlike a regular cache, this shared memory is directly addressable and acts as both a scratchpad and a means of efficiently passing data between threads in an SM. The amount of shared memory utilized affects the potential **occupancy**, the maximum number of blocks that can be scheduled simultaneously in an SM. Every block in a kernel will request the same amount of shared memory. If the total amount of shared memory is more than the SM can support, the occupancy will be reduced, leading to fewer blocks running in parallel and some threads sitting idle.

To achieve high performance on GPUs, we must design GPU kernels for ANNS index construction and querying that efficiently utilize shared memory to maximize occupancy. Specifically, we aim to keep all frequently used data in shared memory and carefully select data structures that fit within the available resources without reducing maximum occupancy.

2.3 Roofline model

The roofline model [39] is a simple, quantitative performance model that bounds the attainable performance of an application on a given architecture using two hardware limits: peak compute throughput and peak memory bandwidth. Performance is expressed as a function of *arithmetic intensity*, defined as the ratio of useful operations to bytes transferred from main memory. For low arithmetic intensity kernels, performance is limited by memory bandwidth and grows linearly with arithmetic intensity; for high intensity kernels, performance saturates at the hardware’s peak compute rate. Graphically, these bounds form a “roofline” (see Figure 1b): a sloped bandwidth roof intersecting a flat compute roof, making it easy to see whether a workload is memory-bound or compute-bound and how close it is to hardware limits.

The roofline model is widely used to guide performance optimization and architectural analysis as it abstracts complex microarchitectural details into a small set of measurable parameters. Optimizations that increase data reuse (e.g., blocking, caching, fusion) move kernels rightward by increasing arithmetic intensity, while vectorization, parallelism, and instruction-level efficiency move kernels upward towards the compute roof. Extensions of the model incorporate multiple memory levels, ceilings for specific bottlenecks, and heterogeneous devices, but the core insight remains: achievable performance is fundamentally constrained by the balance between computation

and data movement. This framing has proven effective for reasoning about performance portability across CPUs, GPUs, and accelerators, and for communicating optimization priorities in both systems and data-intensive workloads. *We use the roofline model to evaluate both the achieved and potential performance of ANNS indices on GPUs.*

3 VAMANA INDEX

In this section, we cover the Vamana algorithm graph structure, construction and query algorithm, and the batch-parallel construction algorithm. Our system Jasper employs the Vamana graph [15], a directed proximity graph designed to support efficient greedy search with bounded out-degree, to build the approximate nearest neighbor search (ANNS) index. We choose the Vamana graph as it supports both a fast and accurate greedy search and an efficient parallel construction algorithm introduced in ParlayANN [20]. We describe how we develop GPU-accelerated Vamana index along with several GPU optimizations in the next section.

3.1 Graph definition

The Vamana index is a directed graph $G = (V, E)$ constructed over a set of data vectors $V = \{x_1, \dots, x_N\}$, where N is the total number of vectors. Each node maintains an adjacency list of at most R outgoing edges. A distinguished entry point $s \in V$ is used to initialize both graph construction and query traversal.

The edge set E is selected to ensure that the graph remains sparse while preserving navigability. For a given vertex in the graph and query vector, there is a high probability that one of the outgoing edges of the vertex leads to a vertex that is closer to the query. This property means that greedy search will converge to a set of points close to a target query and is critical for enabling low-latency approximate search.

3.2 Vamana construction algorithm

The original Vamana construction algorithm starts with all vertices contained within a graph with a random set of edges with maximum outgoing degree R . Vamana graph construction proceeds incrementally to refine the graph one vertex at a time. Refinement of vertices proceeds in two phases. First, Vamana uses BEAMSEARCH to identify candidate neighbors in the existing graph for the new vertex. Second, Vamana applies a pruning procedure, ROBUSTPRUNE, to reattach the vertex to the graph while enforcing a strict bound on the out-degree.

Beam search. Given a vector x to be inserted, the construction algorithm performs an approximate nearest neighbor search in the current graph using BEAMSEARCH. The pseudocode for this procedure is shown in Algorithm 1. The search is initialized at a designated start vertex, typically chosen as the *medoid* (the vector closest to the center) of the dataset.

BEAMSEARCH maintains two sets: (i) a *frontier*, which stores the K closest candidate vertices discovered so far, ordered by increasing distance to the query vector x , and (ii) a *visited list*, which records all vertices whose outgoing edges have been explored. At each iteration, the algorithm selects the closest vertex in the frontier that has not yet been visited, loads its outgoing edges, computes the distance between x and each neighbor, and inserts newly encountered vertices into the frontier.

If the size of the frontier exceeds the beam width K , the furthest candidates are discarded. This expansion process continues until

Algorithm 1: BeamSearch (DiskANN)

```

Input: Graph  $G$ ,  

       query vector  $q$ , beam width  $K$ , start vertex  $m$  (medoid)  

Output: Frontier  $F$  of  $K$  nearest neighbors, visited set  $V$   

 $F \leftarrow \{m\}$  (priority queue by distance)  

 $V \leftarrow \emptyset$   

while there exists an unvisited vertex  $u \in F$  do  

  Mark  $u$  visited:  $V \leftarrow V \cup \{u\}$   

  for each neighbor  $v$  of  $u$  do  

    if  $v \notin V$  then  

      Compute distance  $d(q, v)$   

      Insert  $v$  into  $F$  with priority  $d(q, v)$   

    if  $|F| > K$  then  

      Remove furthest elements from  $F$  until  $|F| = K$   

return  $(F, V)$ 

```

all vertices in the frontier have been visited. The procedure returns both the final frontier, representing approximate nearest neighbors of x , and the full visited list, which captures the local search region explored during insertion.

Edge attachment. Once BEAMSEARCH completes, the new vertex x is attached to the graph using the vertices in the visited list. Initially, bidirectional edges are added between x and each vertex in the visited list, temporarily allowing the out-degree of affected vertices to exceed the maximum degree bound R .

Algorithm 2: RobustPrune (DiskANN)

```

Input: Node  $p$ , candidate neighbors  

        $N(p)$ , degree cap  $R$ , pruning factor  $\alpha$ , distance  $d$   

Output: Pruned neighbor set  $N'(p)$   

Sort  $N(p)$  by  $d(p, \cdot)$  (closest first)  

 $N'(p) \leftarrow \emptyset$  (initialize as empty);  

while  $|N'(p)| < R$  and  $N(p)$  not empty do  

   $p^* \leftarrow$  extract closest from  $N(p)$   

  Add  $p^*$  to  $N'(p)$   

  for each  $p' \in N(p)$  do  

    if  $\alpha \cdot d(p^*, p') \leq d(p, p')$  then  

      Discard  $p'$  from  $N(p)$   

    else  

      Keep  $p'$  in  $N(p)$   

return  $N'(p)$ 

```

Robust prune. To restore the degree bound, Vamana applies the ROBUSTPRUNE procedure to any vertex whose outgoing edge list exceeds R (maximum out degree). The pseudocode for this procedure is shown in Algorithm 2. Given a vertex p , ROBUSTPRUNE takes the current set of outgoing neighbors and sorts them by increasing distance from p . The algorithm iteratively selects the closest remaining neighbor p^* and adds it to the pruned adjacency list. For each remaining candidate neighbor p' , ROBUSTPRUNE compares the distance $d(p^*, p')$ to the distance $d(p, p')$. If

$$\alpha \cdot d(p^*, p') \leq d(p, p'),$$

then p' is removed from consideration. This process repeats until either the pruned adjacency list reaches size R or no candidates remain.

Intuitively, **ROBUSTPRUNE** removes edges that are redundant due to the existence of a strong two-hop path: a direct edge from p to p' is discarded if p' can be reached via a significantly closer neighbor p^* . The parameter $\alpha > 1$ controls the aggressiveness of pruning and trades off graph sparsity for navigability.

Together, **BEAMSEARCH** and **ROBUSTPRUNE** allow Vamana to incrementally construct a bounded-degree proximity graph that preserves long-range connectivity while supporting efficient greedy traversal during query time.

3.3 ParlayANN

ParlayANN [20] is an extension of the Vamana construction algorithm that addresses a fundamental scalability bottleneck in parallel graph construction by adopting a batch-parallel insertion scheme. While the original DiskANN [15] algorithm supports inserting points in parallel, it relies on fine-grained locks to update adjacency lists. In practice, this design leads to significant contention on high-centrality vertices, such as the *medoid*. During the greedy search, high-centrality vertices are frequently traversed, and concurrent insertions attempt to add edges to these vertices simultaneously, resulting in serialization that limits parallel scalability.

ParlayANN eliminates this bottleneck by replacing lock-based updates with a lock-free, batch-parallel construction strategy. The core idea is to decouple graph traversal from graph mutation, allowing expensive updates to be applied in parallel without contention.

Algorithm 3: Batch Insertion (ParlayANN)

```

Input: Batch of new points
       $B$ , current graph  $G$ , beam width  $K$ , degree cap  $R$ 
Output: Graph  $G$  updated with  $B$ 
Step 1: Local candidate generation
  for each  $x \in B$  do in parallel
     $(F, V) \leftarrow \text{BeamSearch}(G, x, K, G.\text{medoid})$ 
     $E_x \leftarrow \{(x, v) : v \in V\}$       // add edges for new nodes
Step 2: Global edge collection
   $E \leftarrow \bigcup_{x \in B} E_x$           // concatenate edges
Step 3: Semisort and parallel pruning
  Group  $E$  by endpoint using Semisort
  for each vertex  $u$  touched by  $E$  do in parallel
     $N'(u) \leftarrow \text{RobustPrune}(u, N(u) \cup E[u], R)$ 
    Update adjacency list of  $u$  with  $N'(u)$ 
  return  $G$ 

```

ParlayANN restructures graph construction (Algorithm 3) into two distinct, parallelizable phases. In the first phase, **BEAMSEARCH** (Algorithm 1) is executed independently and in parallel for each vertex to be inserted. Each search operates on a read-only snapshot of the current graph and produces a set of candidate edges corresponding to the vertices encountered during traversal. Importantly, no adjacency lists are modified during this phase.

Instead of applying updates immediately, all candidate edges produced by the batch are written to a temporary edge collection. This collection is then *semisorted*, grouping edges by their target vertex at

substantially lower cost than a full sort. Semisort guarantees that all candidate edges incident to a given vertex are co-located, enabling subsequent processing to be performed independently per vertex.

In the second phase, **ROBUSTPRUNE** (Algorithm 2) is applied in a batch-parallel design. Each vertex that has received new candidate edges is assigned a unique thread, which merges the proposed edges with the existing adjacency list and applies **ROBUSTPRUNE** to enforce the maximum out-degree constraint R . Because all edges incident to a vertex are processed by a single thread, this phase requires no locks or cross-thread synchronization.

This lock-free design removes contention around centrally located vertices and allows ParlayANN to efficiently exploit multicore parallelism. The key insight is that the pruning step, which determines the final neighborhood structure and dominates construction cost, can be fully decoupled from concurrent graph traversals by deferring updates and processing them in parallel batches. As a result, ParlayANN achieves significantly faster index construction while preserving the structural guarantees of the Vamana graph and maintaining comparable query performance and accuracy.

3.4 Why is the Vamana appropriate for GPUs?

Compared to many alternative ANN indices, the Vamana graph offers a high degree of parallelism across both index construction and query execution, enabling efficient use of modern GPUs. Its construction is inherently parallel: vertices are processed independently, each following a predictable sequence of steps that minimizes thread divergence. Distance computations and graph traversal both expose fine-grained parallelism. Vamana also supports efficient incremental updates. Each insertion performs a bounded beam search over a small subset of vertices and adds at most 2R edges, keeping overhead predictable. By comparison, update procedures for methods such as NN-Descent can be substantially more expensive, as multiple refinement rounds are required and any visited node may become a neighbor. Prior work shows that Vamana matches or exceeds alternative graph indices in search quality across diverse datasets, making it a strong foundation for high-performance, updatable ANNS [15].

4 JASPER: A GPU NATIVE ANNS SYSTEM

This section presents the design of Jasper. The central challenge in GPU-based ANNS is sustaining high hardware (compute and memory) utilization for an irregular, data-dependent, and memory-intensive workload. Existing systems trade off compute efficiency for memory bandwidth, or vice versa. Jasper achieves both simultaneously by re-architecting greedy beam search and its associated data structures around GPU execution constraints.

We first describe how we navigate and overcome the trade-off between compute and memory utilization, new GPU-native optimizations to the ParlayANN design, GPU kernel design in Jasper, and how we design batch-parallel construction.

4.1 Block-per-query execution model

A central design decision in Jasper is to assign one CUDA thread block to each query or inserted vector. This block-per-query model allows threads to cooperatively execute search while keeping all per-query state (frontier, candidates, distances) in shared memory, reducing global memory traffic and enabling data reuse. Computing distances

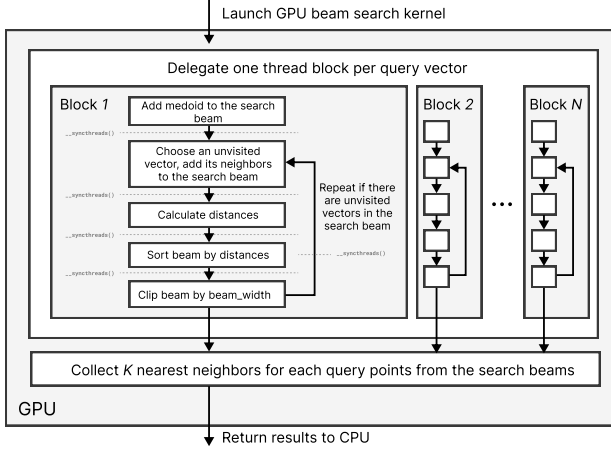


Figure 2: ANNS query pipeline in Jasper.

between vectors is embarrassingly parallel and occupies the full block, while irregular phases such as candidate expansion and graph traversal are partially serialized to reduce control-flow divergence.

The size of the thread block controls a trade-off between per-query compute throughput and the number of memory requests issued. Larger blocks increase arithmetic throughput, instruction-level parallelism, and shared-memory capacity per query, while smaller blocks allow more concurrent queries in each SM (streaming multiprocessor), allowing for higher memory utilization. The optimal trade-off choice depends on the compute and memory balance of the distance kernel. For low-dimensional datasets such as BigANN, where performance is memory-bound, smaller blocks maximize throughput. For high-dimensional datasets such as Gist, where distance computation dominates (17.6× higher cost than BigANN), larger blocks that maximize per-query parallelism achieve higher throughput. In summary, *smaller vectors favor higher query concurrency; larger vectors require greater per-query compute resources*.

4.2 Divergence from ParlayANN construction

Our version of BEAMSEARCH diverges from ParlayANN’s BEAMSEARCH due to the difference between CPU and GPU parallelism. We are limited by the computing model and resources when running BEAMSEARCH on GPU. The BEAMSEARCH algorithm in ParlayANN is serial for each query, as there are many more queries than CPU threads. On the GPU, we have an order of magnitude more threads. To fully saturate the GPU compute and achieve high performance, we must parallelize the internal components of BEAMSEARCH.

Different hash table choices. A major source of divergence arises from ParlayANN’s use of a lossy hash table during beam search. The original algorithm employs a fixed-size (512-slot) hash table with direct replacement to track previously visited vertices and prune duplicates. On CPUs, this structure is accessed sequentially within a single thread, yielding deterministic behavior. On GPUs, preserving this access pattern would require serializing hash table operations across cooperating threads, severely limiting throughput. Parallelizing these operations improves performance but introduces non-determinism. We find that this hash table does not significantly

affect accuracy or search throughput on the GPU. Removing the hash table reduces shared memory pressure and allows Jasper to schedule more queries per block.

Different merge order. Jasper employs a different candidate merge order during beam search. ParlayANN implements a deferred-merge optimization, which postpones sorting and merging when candidate lists are smaller than a fixed fraction of the beam width. The size of the candidate set depends on the results of the hash table lookup: with non-deterministic hash tables, we cannot guarantee this mechanism produces the same candidate list order each time. Empirically, we find that removing the hash table and deferred merging materially affects neither index quality or query accuracy. Consequently, Jasper removes both features. This simplifies control flow, preserves determinism, and eliminates a major source of thread divergence.

4.3 Optimizing BEAMSEARCH for GPUs

We now describe the low-level kernel optimizations used to adapt greedy beam search to the GPU execution model. We focus on reducing redundant arithmetic intensity, improving memory efficiency, and maximizing parallel utilization within each thread block, enabling distance evaluation and candidate processing to approach the hardware limits of modern GPUs.

Optimizing distance calculations. We observe that the square root operation accounts for over 40% of Euclidean distance computation time. Since square root is monotonic over the non-negative reals, we safely elide it and compare squared distances instead, preserving correctness while significantly reducing compute overhead.

Optimizing beam search through kernel fusion. We further reduce overhead by fusing distance computation, frontier sorting, and neighbor expansion into a single kernel executed by one thread block per query. Please refer to Figure 2. Kernel fusion eliminates repeated launch overhead and allows all intermediate data to remain in shared memory, improving both latency and bandwidth utilization, similar to the approach used in CAGRA [25].

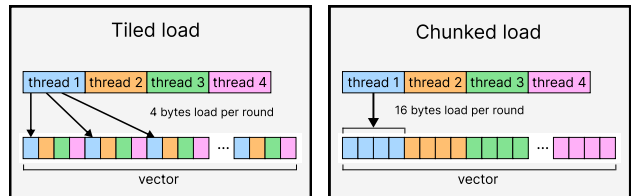


Figure 3: Comparison of the two different load strategies tested in Jasper: tiled loads load one object per thread in the tile at a time, whereas the chunked load strategy loads a fixed amount of data (16 bytes) per thread and has each thread work on all objects loaded in that chunk.

4.4 Vector load optimization

Efficient distance computation is limited not only by arithmetic throughput but also by the memory load latency. By default, when a warp accesses a large object, the compiler emits a sequence of 16-byte loads issued by a single thread, which limits latency hiding. Element-wise loads distribute requests across threads but reduce effective bandwidth, as each element is no more than 4 bytes large.

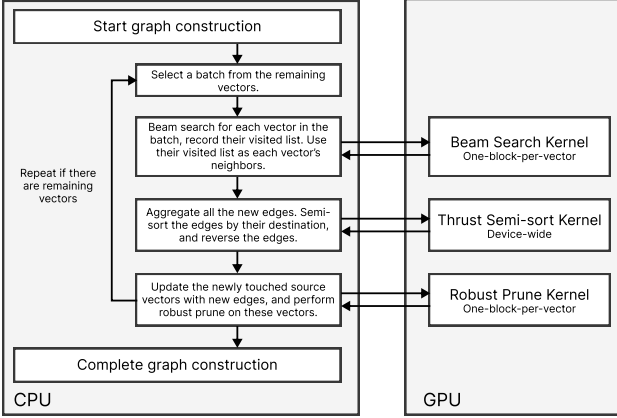


Figure 4: Batch graph construction pipeline in Jasper.

We adopt a *chunked loading scheme* that partitions each vector into 16-byte segments and assigns one segment to each thread. Threads load query and candidate chunks in parallel, compute partial distances locally, and iterate until the full vector is processed. A block-wide reduction then produces the final distance. This approach issues many coalesced 16-byte loads simultaneously to achieve near-peak memory bandwidth.

Figure 3 shows the difference between tiled and chunked loading. Chunked loading improves performance for latency-sensitive workloads: for small beam widths, where search is memory latency bound, it yields up to a 14% speedup. For large beam widths, where compute throughput dominates, optimized loads match baseline performance without loss.

4.5 Batch construction on GPUs

To support high-throughput index construction, Jasper adopts the bulk construction algorithm. ParlayANN relies on fork-join parallelism (via ParlayLib [6]) and a semisort to group edges before insertion, enabling lock-free parallel updates. Fork-join dynamically decomposes large tasks (e.g., sorting and grouping edges) into smaller subtasks that are scheduled across CPU threads.

ParlayANN’s execution model does not map directly to GPUs: kernel launches require a fixed thread configuration, dynamic task spawning is not supported within a kernel, and excessive kernel launches incur substantial overhead. We therefore fuse *search*, *grouping*, and *pruning* into a small number of self-contained GPU kernels with fixed parallel structure. Please refer to Figure 4. Although this removes some scheduling flexibility, it preserves the scalability of batch-parallel search and pruning while conforming to the GPU execution model and minimizing launch overhead.

GPU-efficient pruning. We implement a hybrid pruning strategy for ROBUSTPRUNE. Outgoing edges produced by beam search are accumulated together with existing edges that require pruning and are stored in a unified buffer. This buffer is fully sorted by vertex ID and distance using the CUDA Thrust library. While ParlayANN performs a semisort followed by per-vertex distance sorting using a single thread, we find that on GPUs a full parallel sort provides

better load balance, as individual threads are relatively weak and uneven work distribution is costly.

After sorting, each vertex’s edge list is pruned by assigning an entire SM (1024 threads) to the operation. ROBUSTPRUNE is dominated by distance computations and therefore benefits from high intra-vertex parallelism.

4.6 Scalability with batch size for updates

Index construction in Jasper is performed entirely on the GPU: both the dataset vectors and the evolving graph reside in device memory, eliminating PCIe transfers and using the remaining memory as workspace for batch processing. The achievable batch size is therefore constrained by the available device memory after storing the index and directly determines the degree of parallelism and throughput of the construction pipeline.

On an NVIDIA A100 with 80 GB of memory, the BigANN-100M dataset and its graph occupy 38.5 GB, leaving 41.5 GB for construction buffers; this supports an optimal batch size of approximately 1M vectors. For Deep-100M, the index occupies 64.1 GB, leaving 15.9 GB of workspace and an optimal batch size of approximately 400K vectors. These batch sizes maximize construction throughput by fully utilizing available device memory while keeping all computation and data movement on the GPU.

5 VECTOR QUANTIZATION

Modern embedding models produce vectors spanning hundreds to thousands of dimensions, with per-vector sizes ranging from 96 bytes to over 6000 bytes as shown in BigANN benchmarks [30]. ANNS is memory-bound: each vector element is read once, used for a single arithmetic operation, and discarded. Reducing vector size directly improves query throughput.

To reduce per-vector storage and I/O costs while preserving search accuracy, we consider *quantization*, which compresses vectors while approximately preserving distances. The most widely used approach for ANNS is *product quantization* (PQ) [17]. PQ divides each vector into K disjoint subvectors and quantizes each independently using a small codebook of 256 centroids. Each subvector is then encoded as a single byte indicating its nearest centroid, compressing a high-dimensional vector to just K bytes. Distance computation uses a precomputed *lookup table* storing centroid-to-centroid distances for each subspace. This results in significant compression with modest accuracy loss, as error arises only from the approximation of each subvector by its nearest centroid.

Although PQ compresses vectors effectively, its *lookup table* access pattern results in lower throughput on GPUs. GPU memory is organized into 32-byte *sectors* that are loaded atomically—reading a single 4-byte distance entry wastes the remaining 28 bytes, causing 8× read amplification. A straightforward solution is to place the lookup table in shared memory, but even a modest configuration ($K = 32$) requires $32 \times 256 \times 256 \times 4$ bytes (8 MB), far exceeding shared memory capacity. We implemented PQ in Jasper but found that throughput was strictly worse than unquantized search for all configurations tested. Similar conclusions regarding the PQ performance on GPU has been presented in prior research [25].

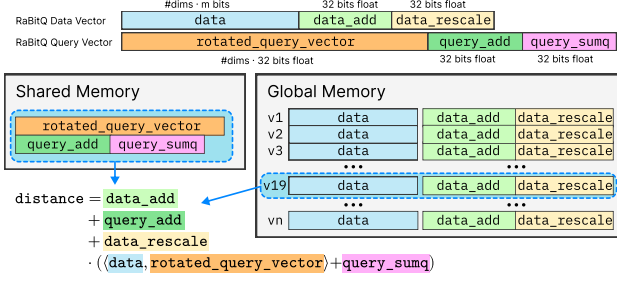


Figure 5: During L2 distance calculation, RaBitQ loads query vector and its metadata from shared memory, and it loads quantized data vector and its metadata from global memory.

5.1 RaBitQ quantization

To effectively use quantization on the GPU, we must avoid random memory accesses during distance computation. Previous GPU implementations treat quantization as a trade-off: smaller vectors and lower memory I/O at the cost of lower throughput [25, 35]. We show this trade-off is not fundamental. Jasper employs RaBitQ [11], a quantization method that is well suited for GPUs. RaBitQ requires only sequential memory access, simple arithmetic, and requires no lookup tables.

RaBitQ estimates the distance using the inner product between the quantized data vector with the query vector. We define the following variables: m is the number of quantized bits per dimension, c is the centroid vector, v is the original data vector, q is the original query vector, o is the rotated and normalized data vector $v - c$, \bar{o} is the quantized data vector, and Δ_x is the rescaling factor of \bar{o} from o .

During data quantization, RaBitQ compresses the data vectors by first normalizing them and applying a random rotation matrix. With high dimensional vectors, any rotated dimensions are likely tightly clustered around 0: according to the Johnson-Lindenstrauss lemma [16], the value of any coordinate is no further than $\frac{2}{\sqrt{D}}$ away from 0 with high probability. This allows RaBitQ to treat each dimension as an unbiased distribution and enables simple scalar quantization. RaBitQ encodes each dimension with m bits along with two floating point metadata: `data_add` and `data_rescale`, where they correspond to $\|v - c\|^2 + 2 \cdot \|v - c\|^2 \cdot \frac{\langle c, o \rangle}{\langle o, o \rangle}$ and $-2 \frac{\Delta_x}{\langle o, o \rangle}$. These precomputed values save computation during distance estimation. In total, the size of the quantized vector is $\# \text{dims} \cdot m \text{ bits} + 2 \cdot \text{sizeof}(\text{float})$.

During querying, RaBitQ applies the same rotation matrix to the query vector, and RaBitQ calculates each query vector's metadata: `query_add` and `query_sumq`, where they correspond to $\|q - c\|^2$ and $\sum (q - c) \cdot \frac{2^{m-1} - 1}{2}$. Figure 5 shows how RaBitQ estimates distances solely based on quantized vectors and rotated query vectors. The RaBitQ estimator reduces the L2 distance calculation to estimating the inner product between the quantized data vector (`data`) and rotated query vector (`rotated_query_vector`). This process estimates the vector distance without branching or randomized memory accesses while most of the values are pre-computed, which makes it highly suitable for GPU execution. RaBitQ's sequential memory access during distance calculation also allows us to utilize the same loading technique for exact vector loading in Section 6.6.

Name	Data Type	Dimensions	Distance Type	Size
BigANN	uint8	128	Euclidean	100M
Deep	float32	96	Euclidean	100M
Gist	float32	960	Euclidean	1M
OpenAI-ArXiv	float32	1536	Euclidean	2.3M
Yandex Text-to-Image	float32	200	Inner product	10M

Table 1: Details of datasets employed in our evaluation.

Jasper integrates GPU-accelerated RaBitQ. RaBitQ achieves 2 \times compression for 8-bit vectors and up to 8 \times for 32-bit vectors. On datasets with large dimensions, our results demonstrate that Jasper with RaBitQ performs significantly better than our exact distance calculation version. In Section 6.6, we perform a detailed analysis between RaBitQ's performance and PQ's performance.

6 EVALUATION

In this section, we evaluate the performance of Jasper against four state-of-the-art ANNS indices: three GPU-based and one CPU-based index. We evaluate the construction, query, and update performance across five real-world datasets varying in size and number of dimensions. We further evaluate the effectiveness of Jasper in saturating GPU resources using the roofline model [39]. Finally, we perform a series of micro-benchmarks to evaluate the impact of various GPU-specific optimizations introduced in Jasper and discuss how these are broadly applicable for optimizing other GPU-accelerated systems.

6.1 Experimental setup

We evaluate all systems on along three dimensions:

- **Construction throughput:** measured as the total time required to build the index used in subsequent experiments.
- **Query throughput:** reported as the number of ANN queries completed per second.
- **Recall:** which measures the accuracy of the Top- K results and is defined as $\text{Recall}@K = \frac{\# \text{ of exact Top-}K \text{ results returned}}{K}$. We report recall at 1@1, 10@10, 50@50, and 100@100.

Hardware. All CPU experiments are conducted on an Intel(R) Xeon(R) Gold 5218 CPU with 32 physical cores (64 hardware threads) at 2.30 GHz. GPU experiments are run on an NVIDIA A100 (SM80) with 80 GB of HBM memory using CUDA 12.9.

Datasets. For evaluation, we select the following datasets taken from the Big_ANN_Benchmarks [30] repository, summarized in Table 1.

- BigANN: 100 million 128-dimensional uint8 vectors with Euclidean distance from the SIFT collection. There are 10K vectors in the test set.
- Deep/Yandex: 100 million PCA-reduced, normalized GoogLeNet embeddings (96-dimensional float32). Euclidean distance and 10K queries.
- Gist: 1 million 960-dimensional float32 vectors with euclidean distance and 1K query vectors in the test set.
- OpenAI-ArXiv: 2.3 million 1536-dimensional float32 embeddings of Arxiv papers. Query set is 10K vectors.
- Text2Image: 10 million 200-dimensional float32 image embeddings from the Se-ResNext-101 model. Distance is maximum inner product search (MIPS) and there are 10K queries in the test set.

Dataset	Jasper	CAGRA	ParlayANN	GANNS	Jasper Speedup over CAGRA
BigANN	679.8	1323.3	1418.2	-	1.95×
Deep	785.0	825.6	4336.9	-	1.05×
Gist	14.8	14.1	210.6	151.9	0.95×
OpenAI	120.1	127.8	1379.4	899.2	1.06×
Text2Image	88.7	619.2	184.0	1017.4	6.98×

Table 2: Index construction time in seconds for various ANNS indexes. ParlayANN is constructed on CPU. GANNS could not finish construction on BigANN and Deep 100M datasets.

ANNS indices. We compare Jasper to the following ANNS indices:

- **CAGRA** [25]: The state-of-the-art in GPU index construction. CAGRA constructs a graph index using NN-Descent [36]. NN-Descent iteratively improves graph connectivity by expanding each node’s neighborhood through 2-hop neighbors. The resulting graph is well-connected but too dense for GPU memory. CAGRA addresses this with a three-phase pruning algorithm: edges are sorted by length, redundant edges with good 2-hop alternatives are removed, and finally the graph is merged with its reverse and pruned again to produce the final index.
- **BANG** [35]: BANG extends the query execution of DiskANN [15] to GPUs. BANG does not perform construction and requires a pre-constructed Vamama graph from DiskANN. It uses product quantization to reduce the size of the vectors. The quantized vectors are stored in the GPU memory while the graph and full vector data are stored in DRAM. The entirety of a streaming multiprocessor (SM) is used for each query. One thread is used for each distance calculation, as distances can be calculated using only PQ table lookups. To process queries more efficiently, Bloom filters are used to represent the visited list, lowering the memory requirements for searching.
- **GANNS**: GANNS [41] is an implementation of the HNSW graph algorithm optimized for GPUs. To optimize for GPU execution, GANNS uses lazy data structures - rather than maintain a priority queue, GANNS maintains two lists (frontier and visited) and only occasionally updates the lists to mark vertices as visited. They avoid the use of a hash table for marking visited vertices during queries, and use multiple thread blocks per query. The construction algorithm for HNSW graphs is difficult to parallelize, so GANNS constructs many small graphs in parallel and then sequentially merges them. GANNS does not support dataset with 100 million vectors.
- **ParlayANN**: ParlayANN is the state of the art CPU ANNS system. It implements Vamana for construction and implements the batch-parallel construction algorithm. This algorithm is discussed in more detail in Section 3.3. ParlayANN has the ability to perform *scalar* quantization in which floats are translated directly into smaller integer types by evenly bucketing the real number line into buckets of a size Δ based on the integer size.

For all indices the graph size is held constant at $R=64$, so each vertex has at most 64 outgoing edges.

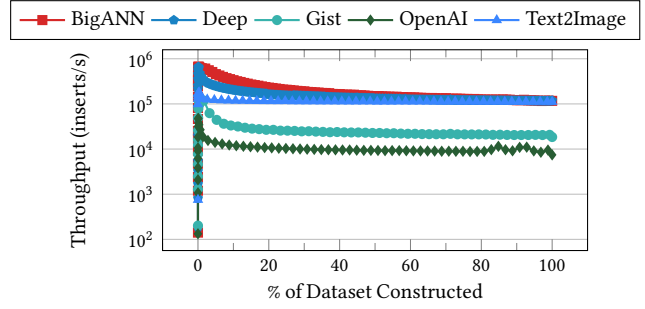


Figure 6: Jasper incremental construction throughput. X-axis is the % of the dataset constructed so far, with each data point being the throughput for one batch. Y-axis is throughput on a log-scale, higher is better.

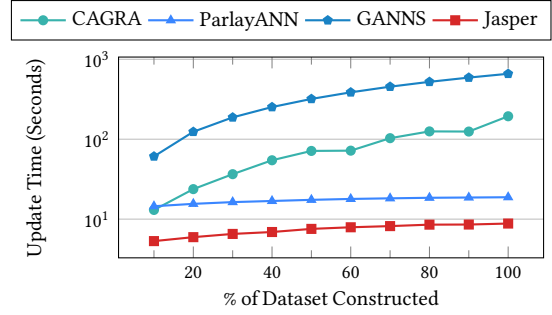


Figure 7: Incremental vs non-incremental construction throughput for BigANN 10M. Jasper and ParlayANN support batch incremental updates. CAGRA and GANNS do not support updates and need to be built from scratch at each step. X-axis is percentage of dataset constructed and each data point is a further $\frac{1}{10}$ th of dataset constructed. Y-axis is on log-scale, lower is better.

6.2 Index construction

Here we evaluate the index construction performance of Jasper against other ANNS indexes.

Bulk construction. In this benchmark, datasets are constructed in one shot. Results are shown in Table 2. We measure the overall construction throughput as the ratio of the number of vectors indexed and total construction time. Jasper achieves the highest construction throughput on all datasets except Gist, with peak throughput of 674K inserts/sec on BigANN. CAGRA is the fastest dataset for Gist construction with peak throughput of 70.6K inserts/sec. Jasper has comparable speed with CAGRA when constructing Gist. However, due to the smaller number of vectors in Gist (1 million), the construction batch size for Jasper is bounded to 2% of the total dataset, resulting in under-utilization of GPU parallelism. ParlayANN while running on CPU (64 threads) is between 2–14× slower than Jasper. GANNS is another GPU-based ANNS index but is between 7–11× slower than Jasper. Additionally, GANNS does not support construction on 100M datasets as it is constrained due to `int32` datatype being employed to index into the vector array. 100M vectors with 128/96 dimensions require 64-bit datatype for indexing.

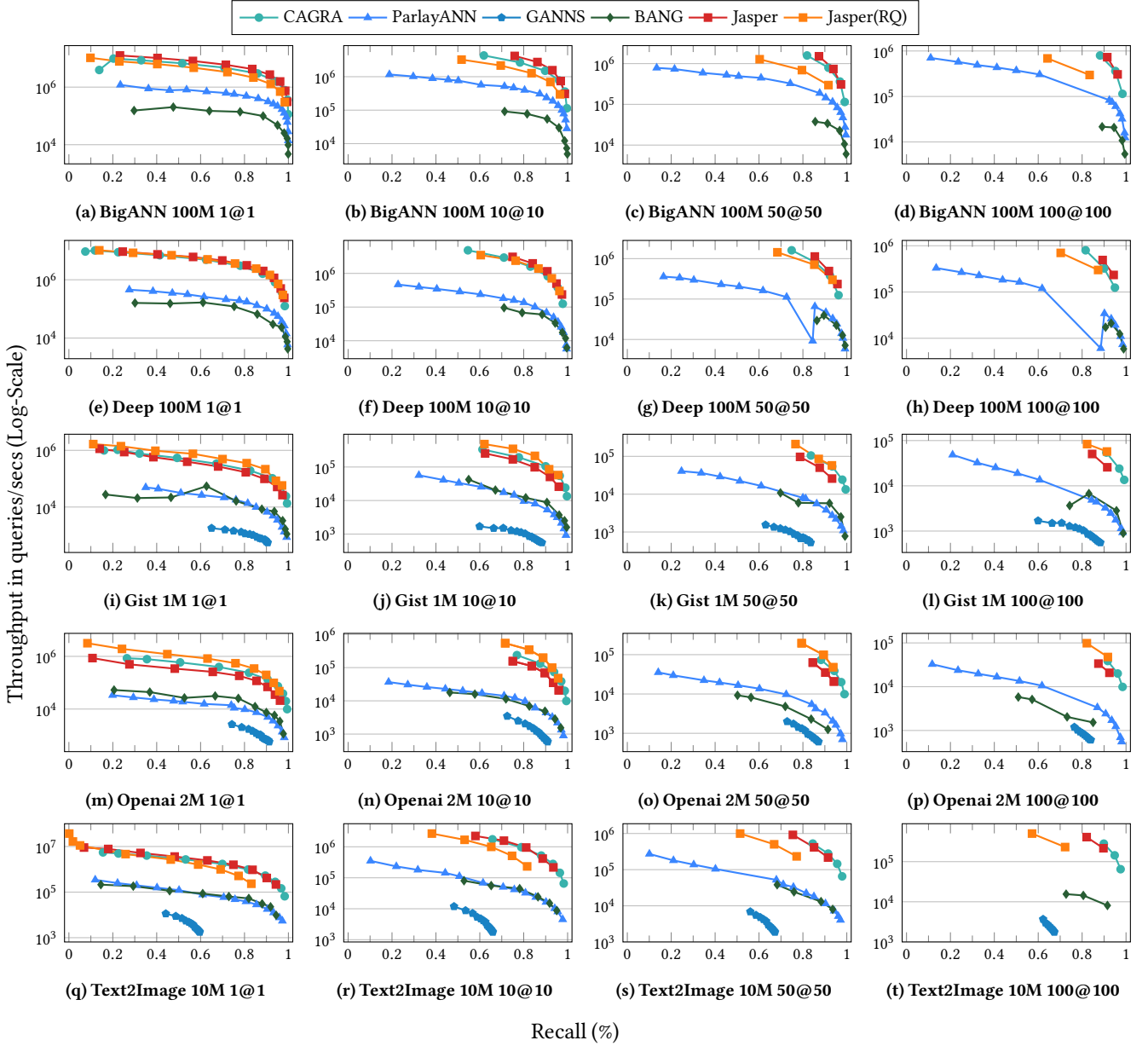


Figure 8: Query recall/throughput curves for various ANNS indexes across five datasets on Nvidia A100 GPU. We report recall at 1@1, 10@10, 50@50, and 100@100. Y-axis is on log-scale. X-axis is recall. Higher and more to the right is better.

Incremental construction. Figure 6 shows how Jasper’s construction throughput changes as the index grows. We build the index incrementally, inserting vectors in batches of 2% of the total dataset. Across all datasets, throughput decreases as the index grows, but the slowdown is sub-linear in index size. For example, on Deep, Jasper inserts 251K vectors/sec when the index is at 5% capacity (500K vectors). When the index reaches 99% capacity (9.9 million vectors), throughput drops to 116K vectors/sec. This is less than a 2.2 \times slowdown despite a 20 \times increase in index size, demonstrating that Jasper maintains efficient insertion performance even as the index grows large.

Figure 7 illustrates why incremental construction matters. We measure the time required to add a 10% slice of new vectors to an already-constructed index, simulating a common production scenario where new data arrives after the initial index is built. Jasper and ParlayANN, which support incremental updates, complete this operation an order of magnitude faster than CAGRA and GANNS. The difference arises because CAGRA and GANNS lack incremental update support: each batch of new vectors requires rebuilding the entire index from scratch.

6.3 Queries

Here we evaluate the approximate nearest neighbor search (ANNS) performance of Jasper against other ANNS indexes.

Low-dimensional vector datasets: BigANN and Deep. For the low-dimensional vector datasets, Jasper is the fastest index for all recall values supported, with peak throughput of 13.2 million queries / sec at .31 recall. On BigANN, it is followed by Jasper RaBitQ which has the second highest throughput. Jasper is the fastest ANNS index up to .9943 recall as it does not achieve an accuracy higher than that on BigANN. For Deep, CAGRA is the second fastest index for all recall values tested. CAGRA achieves a higher maximum accuracy on these datasets, with peak accuracy of .9999 for BigANN 1@1 and .983 for Deep 1@1.

Jasper is the fastest for the low-dimensional vector datasets due to its optimized vector loads. For small beam sizes, latency hiding is not as effective as there is relatively little work performed per vector. This means that reducing latency of loads improves the performance of these kernels, as GPU compute spends less time waiting..

High-dimensional vector datasets: Gist and OpenAI. On the high-dimensional vector datasets Gist and OpenAI, distance calculations dominate the run time. To measure the cost of operations, we add cycle counters to every operation in the search kernel. When running Jasper exact on both BigANN and Gist, we see a $17.8\times$ increase in the cycles taken for distance calculations in Gist, with distance calculations becoming the most expensive operation in the entire search.

The large vector size of these datasets benefits quantization as it can reduce the compute and memory requirements of distance calculations. On these datasets, Jasper RaBitQ is the fastest algorithm for all sizes it supports, with peak throughput over 3 million queries/secs and recall up to .94 for 50@50. After Jasper RaBitQ, CAGRA has the second best throughput-recall trade-off curve for all $k@k$ recall curves, followed by Jasper, then ParlayANN and BANG, and finally GANNS.

All indices suffer significant performance reductions on these datasets due to the high volume of data transfers and distance calculations. On these datasets, the use of quantization results in an 8 \times decrease in memory transfer due to reduced vector size. The results in Figure 12 confirm our hypothesis that direct vector comparison is necessary for efficient quantized performance on GPUs: all versions of CAGRA PQ benchmarked against do not show improvements in performance, while Jasper RaBitQ is up to 60% faster than the exact implementation.

Text2Image. Text2Image uses maximal inner product (MIPS) MIPS for distance instead of Euclidean. This makes construction and querying this dataset difficult as MIPS does not preserve the triangle inequality. Having a triangle inequality is necessary for the space to be metric and is crucial in constructing good search graphs using the Vamana indexing method. Without this property, graph construction can have poor results as there is no correlation between the neighbors of a given vector: it is possible to be "close" to a target query vertex and "far" from all of its neighbors, making pruning impossible. To overcome this, ANNS indices convert MIPS into a Euclidean space by adding one extra dimension. This allows for graph construction but comes at the cost of one extra dimension.

Both the Jasper and Jasper RaBitQ implementations suffer from reduced performance on this dataset, as the conversion from MIPS

	Beam width=1			Beam width=256		
	BigANN	Deep	Gist	BigANN	Deep	Gist
Tiled	8.398	6.701	.690	.095	.089	.024
Chunked	9.611	7.622	.769	.095	.089	.024

Table 3: Difference in tiled and chunked load strategies. Table results are throughput in millions of queries per second. For smaller beam widths, the chunked strategy provides lower latency as all load requests are issued simultaneously. For higher beam widths, total memory throughput dominates, resulting in identical performance.

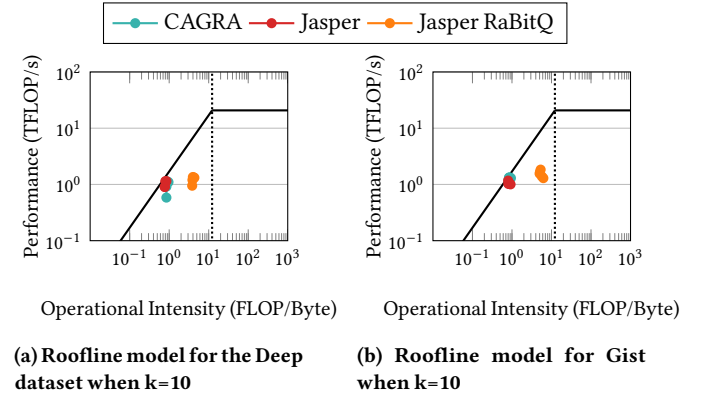


Figure 9: Roofline analysis of the Deep and Gist search kernels for Jasper, Jasper RaBitQ, and CAGRA. Y-axis is on log-scale, higher is better.

to Euclidean distance reduces the accuracy compared to systems like CAGRA that can construct the graph using the original MIPS distance calculation. Jasper has the highest recall/throughput trade-off on this dataset until .9 recall, at which point CAGRA shows the highest recall/throughput trade-off. Due to the low dimensions (200), Jasper exact shows higher performance than Jasper RaBitQ, with Jasper RaBitQ showing reduced recall due to the MIPS distance calculation.

6.4 RaBitQ quantization

Jasper RaBitQ reduces the volume of data loaded during queries, which improves performance on datasets with high-dimensional vectors. As shown in Figure 8, the exact-distance version of Jasper is slower than CAGRA on Gist and OpenAI, but Jasper RaBitQ closes this gap and surpasses CAGRA at the same recalls despite using a lossy representation. For example, on OpenAI at 90% recall (10@10), Jasper RaBitQ is 3 \times faster than Jasper. On Deep, which has smaller vectors, Jasper RaBitQ performs comparably to the exact version.

On datasets with low-dimensional vectors, such as BigANN and Text2Image, Jasper RaBitQ is slightly slower than exact distance computation due to its lossy representation and additional arithmetic overhead. However, Jasper RaBitQ remains valuable in memory-constrained settings because it reduces device memory usage, allowing more vectors to reside on the GPU. We compare Jasper RaBitQ against other quantization methods in Section 6.6.

6.5 Roofline analysis

We use roofline analysis [39] to characterize Jasper’s performance on both low-dimensional (Deep) and high-dimensional (Gist) vectors. Figure 9 compares the arithmetic intensity and achieved throughput of Jasper and Jasper RaBitQ against CAGRA with $K = 10$.

Across both datasets, the roofline results indicate that Jasper operates predominantly in a memory-bound regime, with operational intensities are clustered tightly around 0.7–0.95 FLOP/byte. On DEEP, Jasper achieves peak throughputs around 0.89–1.14 TFLOP/s at these low intensities, closely tracking the sloped bandwidth roof. This behavior is consistent with ANNS workloads dominated by irregular memory accesses during graph traversal, where additional compute cannot be fully exploited without increasing data reuse. The comparable intensity–performance envelope between Jasper and CAGRA on Deep suggests that both systems are similarly constrained by memory bandwidth, with performance differences largely attributable to constant-factor effects such as traversal efficiency and kernel scheduling rather than fundamental compute utilization.

In contrast, Jasper RaBitQ significantly increases operational intensity, where intensities rise to 5.0–6.2 FLOP/byte and achieved performance reaches up to 1.83 TFLOP/s. This rightward shift on the roofline indicates substantially improved arithmetic reuse, allowing Jasper RaBitQ to move closer to the compute roof and escape the strict bandwidth-bound regime observed in Jasper. Overall, these results show that Jasper RaBitQ’s reordering and query-time computation strategies improve performance by reducing memory traffic.

6.6 Microbenchmarks

We now present four microbenchmarks analyzing key design decisions in Jasper. First, we evaluate how tile-based loading affects throughput. Second, we examine the impact of partitioning warps into smaller worker units. Third, we measure how block size affects performance across different vector dimensions. Finally, we compare our RaBitQ implementation against PQ on the GPU.

Load microbenchmark. The load microbenchmark measures performance of our coalesced load implementation against a traditional tiled approach. In this microbenchmark we run both approaches and query BigANN, Deep, and Gist with beam widths 1 and 256, the smallest and largest beam widths supported. The results for this benchmark are in Table 3. For small beam widths, we see that the performance of the coalesced loads is consistently higher than tiled loads. This is due to the reduced latency from issuing load instructions simultaneously. For low beam widths, using coalesced loads provides a 14% performance increase as loads are sent and thus return faster, reducing the latency of the query. For larger beam widths, latency hiding means that total memory bandwidth dominates performance, and the coalesced loads show no measurable change in performance.

Tile microbenchmark. We compare our coalesced load implementation against traditional tiled loading on BigANN, Deep, and Gist using beam widths of 1 and 256 (Table 3). At small beam widths, coalesced loads provide a 14% throughput improvement by issuing all load instructions simultaneously, reducing latency. At large beam widths, sufficient in-flight operations hide memory latency, so both approaches achieve similar throughput.

Block microbenchmark. Block size controls the trade-off between parallelism within a query and the number of concurrent queries per

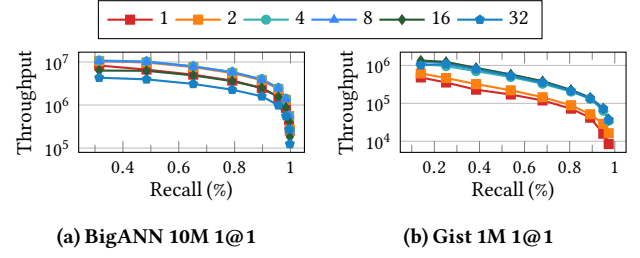


Figure 10: Varying Tile size for BigANN and Gist. Throughput is in millions of queries per second, higher is better.

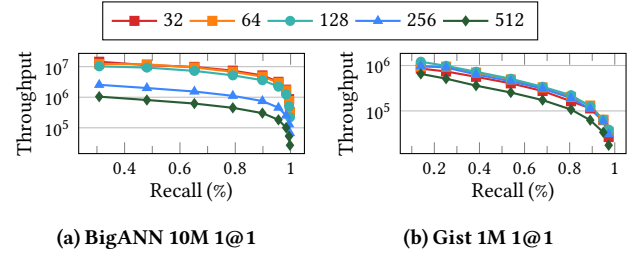


Figure 11: Varying Block size for BigANN and Gist. Throughput is in millions of queries per second, higher is better.

SM. Larger blocks assign more threads to each query; smaller blocks allow more queries to execute simultaneously, increasing memory-level parallelism. Results are shown in Figure 11a and Figure 11b.

For datasets with high-dimensional vectors (Gist, OpenAI), reducing block size improves performance until reaching 128 threads per block. Below this point, performance drops because distance computation becomes the bottleneck—there are too few threads to efficiently process each high-dimensional vector. For datasets with low-dimensional vectors (BigANN, Deep), distance computation is not the bottleneck. Smaller block sizes consistently improve performance by enabling greater memory parallelism. The optimal configuration uses 32 threads per block (a single warp per query), allowing 32 concurrent queries per SM and maximizing memory throughput.

Quantization microbenchmark. We compare quantization methods in Figure 12, measuring query throughput for Jasper (exact and RaBitQ) against CAGRA (exact and PQ) and ParlayANN (exact and 8-bit scalar quantization). To ensure a fair comparison, we evaluate CAGRA’s PQ under two configurations: one matching Jasper RaBitQ’s compression ratio (4× reduction), and one using CAGRA’s default. For ParlayANN’s SQ, we use 8 quantized bits per dimension.

CAGRA’s exact variant is optimized for high-dimensional vectors and slightly outperforms Jasper’s exact computation. However, Jasper RaBitQ outperforms all CAGRA variants, including exact. CAGRA’s PQ achieves throughput similar to its exact version despite reducing memory footprint, the scattered lookups required for PQ distance computation negate any bandwidth savings. These results confirm that RaBitQ is more effective than PQ for GPU workloads. ParlayANN also benefits from reduced memory footprint from quantitation on CPU, showing 3 to 4 times speed up for the same recall compare to ParlayANN exact version.

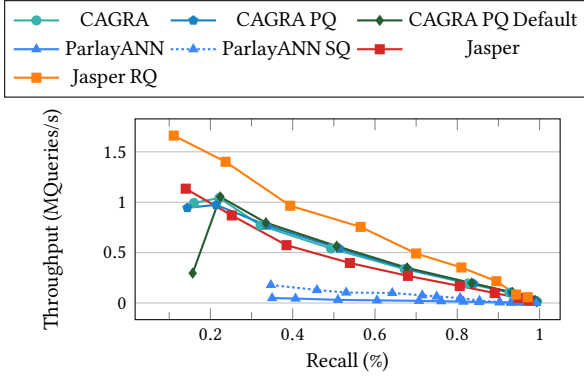


Figure 12: Different quantization method’s query performance for Gist 1M 1@1. X-axis is recall 1@1, Y-axis is throughput in millions of queries per second. Higher and to the right is better.

7 CONCLUSION

In this work, we demonstrate that GPU-native approximate nearest neighbor search (ANNS) can achieve substantial acceleration over CPU variants, enabling high-throughput queries and effective data

co-location with downstream machine learning workloads. We show that the extreme degree of parallelism exposed by modern GPUs introduces new challenges: prior GPU ANNS systems often leave performance on the table due to synchronization overheads and limited shared memory. Our results show that carefully simplifying ANNS kernels to reduce shared memory usage and optimizing data load can significantly increase throughput and achieve higher parallelism.

We demonstrate that Jasper achieves up to 1.93× higher query throughput than CAGRA while providing streaming update capabilities that CAGRA lacks, and delivers 19–131× higher throughput than BANG. Our batch-parallel construction algorithm achieves 2.4× faster index construction than CAGRA on average. Our optimized search kernel achieves 70–80% of peak theoretical throughput.

Our roofline analysis reveals that state-of-the-art GPU ANNS kernels operate close to the memory bandwidth ceiling. Future performance gains must come primarily from reducing data movement, and quantization-aware designs like RaBitQ demonstrate a promising path forward by pushing systems closer to the compute roof where substantial headroom remains.

8 ACKNOWLEDGMENTS

This work is supported by the NSF grant 2517201 and 2513656. Additionally, we would like to thank Harsha Vardhan Simhadri and Magdalén Dobson Manohar for insightful discussions early in the project.

REFERENCES

[1] Philip Adams, Menghao Li, Shi Zhang, Li Tan, Qi Chen, Mingqin Li, Zengzhong Li, Knut Magne Risvik, and Harsha Vardhan Simhadri. 2025. DistributedANN: Efficient Scaling of a Single DiskANN Graph Across Thousands of Computers. In *The 1st Workshop on Vector Databases*. <https://openreview.net/forum?id=6AEsfCLRm3>

[2] Jade Alglave, Mark Batty, Alastair F. Donaldson, Ganesh Gopalakrishnan, Jeroen Ketema, Daniel Poetzl, Tyler Sorensen, and John Wickerson. 2015. GPU Concurrency: Weak Behaviours and Programming Assumptions. In *Proceedings of the Twentieth International Conference on Architectural Support for Programming Languages and Operating Systems* (Istanbul, Turkey) (ASPLOS '15). Association for Computing Machinery, New York, NY, USA, 577–591. doi:10.1145/2694344.2694391

[3] Artem Babenko and Victor Lempitsky. 2015. The Inverted Multi-Index. *IEEE Transactions on Pattern Analysis and Machine Intelligence* 37, 6 (June 2015), 1247–1260. doi:10.1109/tpami.2014.2361319

[4] Iman Belahyane, Mouad Mammas, Hasna Abiou, and Ali Idarrou. 2020. *Graph-Based Image Retrieval: State of the Art*. Springer International Publishing, 299–307. doi:10.1007/978-3-030-51935-3_32

[5] Jon Louis Bentley. 1975. Multidimensional binary search trees used for associative searching. *Commun. ACM* 18, 9 (Sept. 1975), 509–517. doi:10.1145/361002.361007

[6] Guy E. Blelloch, Daniel Anderson, and Laxman Dhulipala. 2020. ParlayLib - A Toolkit for Parallel Algorithms on Shared-Memory Multicore Machines. In *Proceedings of the 32nd ACM Symposium on Parallelism in Algorithms and Architectures (SPAA '20)*. ACM, 507–509. doi:10.1145/3350755.3400254

[7] Mayur Datar, Nicole Immorlica, Piotr Indyk, and Vahab S. Mirrokni. 2004. Locality-sensitive hashing scheme based on p-stable distributions. In *Proceedings of the twentieth annual symposium on Computational geometry (SoCG04)*. ACM, 253–262. doi:10.1145/997817.997857

[8] Wei Dong, Charikar Moses, and Kai Li. 2011. Efficient k-nearest neighbor graph construction for generic similarity measures. In *Proceedings of the 20th international conference on World wide web (WWW '11)*. ACM. doi:10.1145/1963405.1963487

[9] Matthijs Douze, Alexandre Guzhva, Chengqi Deng, Jeff Johnson, Gergely Szilvassy, Pierre-Emmanuel Mazaré, Maria Lomeli, Lucas Hosseini, and Hervé Jégou. 2024. The Faiss library. doi:10.48550/ARXIV.2401.08281

[10] R. A. Finkel and J. L. Bentley. 1974. Quad trees a data structure for retrieval on composite keys. *Acta Informatica* 4, 1 (1974), 1–9. doi:10.1007/bf00288933

[11] Jianyang Gao and Cheng Long. 2024. RaBitQ: Quantizing High-Dimensional Vectors with Theoretical Error Bound for Approximate Nearest Neighbor Search. *Proceedings of the ACM on Management of Data* 2, 3 (May 2024), 1–27. doi:10.1145/3654970

[12] Siddharth Gollapudi, Neel Karia, Varun Sivashankar, Ravishankar Krishnaswamy, Nikit Begwani, Swapnil Raz, Yiyong Lin, Yin Zhang, Neelam Mahapatro, Premkumar Srinivasan, Amit Singh, and Harsha Vardhan Simhadri. 2023. Filtered-DiskANN: Graph Algorithms for Approximate Nearest Neighbor Search with Filters. In *Proceedings of the ACM Web Conference 2023 (WWW '23)*. ACM, 3406–3416. doi:10.1145/3543507.3583552

[13] Xiaoyi Gu, Leman Akoglu, and Alessandro Rinaldo. 2019. Statistical Analysis of Nearest Neighbor Methods for Anomaly Detection. In *Advances in Neural Information Processing Systems*, H. Wallach, H. Larochelle, A. Beygelzimer, F. d'Alché-Buc, E. Fox, and R. Garnett (Eds.), Vol. 32. Curran Associates, Inc. https://proceedings.neurips.cc/paper_files/paper/2019/file/805163a0f0f128e473726ccda5f91bac-Paper.pdf

[14] Piotr Indyk and Rajeev Motwani. 1998. Approximate nearest neighbors: towards removing the curse of dimensionality. In *Proceedings of the thirtieth annual ACM symposium on Theory of computing - STOC '98 (STOC '98)*. ACM Press, 604–613. doi:10.1145/276698.276876

[15] Suhas Jayaram Subramanya, Fnu Devvrit, Harsha Vardhan Simhadri, Ravishankar Krishnaswamy, and Rohan Kadekodi. 2019. DiskANN: Fast Accurate Billion-point Nearest Neighbor Search on a Single Node. In *Advances in Neural Information Processing Systems*, H. Wallach, H. Larochelle, A. Beygelzimer, F. d'Alché-Buc, E. Fox, and R. Garnett (Eds.), Vol. 32. Curran Associates, Inc. <https://proceedings.neurips.cc/paper/2019/file/09853c7fb1d3f8ee67a61b6bf4a78e6-Paper.pdf>

[16] William B. Johnson and Joram Lindenstrauss. 1984. Extensions of Lipschitz mappings into a Hilbert space. 189–206 pages. doi:10.1090/comm/026/737400

[17] H Jégou, M Douze, and C Schmid. 2011. Product Quantization for Nearest Neighbor Search. *IEEE Transactions on Pattern Analysis and Machine Intelligence* 33, 1 (Jan. 2011), 117–128. doi:10.1109/tpami.2010.57

[18] Yury Malkov, Alexander Ponomarenko, Andrey Logvinov, and Vladimir Krylov. 2014. Approximate nearest neighbor algorithm based on navigable small world graphs. *Information Systems* 45 (Sept. 2014), 61–68. doi:10.1016/j.is.2013.10.006

[19] Yu A. Malkov and D. A. Yashunin. 2020. Efficient and Robust Approximate Nearest Neighbor Search Using Hierarchical Navigable Small World Graphs. *IEEE Transactions on Pattern Analysis and Machine Intelligence* 42, 4 (April 2020), 824–836. doi:10.1109/tpami.2018.2889473

[20] Magdalen Dobson Manohar, Zheqi Shen, Guy Blelloch, Laxman Dhulipala, Yan Gu, Harsha Vardhan Simhadri, and Yihan Sun. 2024. ParlayANN: Scalable and Deterministic Parallel Graph-Based Approximate Nearest Neighbor Search Algorithms. In *Proceedings of the 29th ACM SIGPLAN Annual Symposium on Principles and Practice of Parallel Programming (PPoPP '24)*. ACM, 270–285. doi:10.1145/3627535.3638475

[21] Marvin Minsky and Seymour A. Papert. 2017. *Perceptrons: An Introduction to Computational Geometry*. The MIT Press. doi:10.7551/mitpress/11301.001.0001

[22] Rajeev Motwani, Assaf Naor, and Rina Panigrahy. 2008. Lower Bounds on Locality Sensitive Hashing. *SIAM Journal on Discrete Mathematics* 21, 4 (Jan. 2008), 930–935. doi:10.1137/050646858

[23] NVIDIA. 2020. Nvidia A100 tensor core GPU | Data sheet | 1. <https://www.nvidia.com/content/dam/en-zz/Solutions/Data-Center/a100/pdf/nvidia-a100-datasheet-nvidia-us-2188504-web.pdf>

[24] Camilla Birch Okkels, Martin Aumüller, and Arthur Zimek. 2024. *On the Design of Scalable Outlier Detection Methods Using Approximate Nearest Neighbor Graphs*. Springer Nature Switzerland, 170–184. doi:10.1007/978-3-031-75823-2_14

[25] Hiroyuki Ootomo, Akira Naruse, Corey Nolet, Ray Wang, Tamas Feher, and Yong Wang. 2024. CAGRA: Highly Parallel Graph Construction and Approximate Nearest Neighbor Search for GPUs. arXiv:2308.15136 [cs.DS] <https://arxiv.org/abs/2308.15136>

[26] Derrick Quinn, Mohammad Nouri, Neel Patel, John Salihu, Alireza Salemi, Sukhan Lee, Hamed Zamani, and Mohammad Alian. 2025. Accelerating Retrieval-Augmented Generation. In *Proceedings of the 30th ACM International Conference on Architectural Support for Programming Languages and Operating Systems, Volume 1* (Rotterdam, Netherlands) (ASPLOS '25). Association for Computing Machinery, New York, NY, USA, 15–32. doi:Quinn2025

[27] MD Shaikh Rahman, Syed Maudud E Rabbi, and Muhammad Mahbubur Rashid. 2024. Optimizing Domain-Specific Image Retrieval: A Benchmark of FAISS and Annoy with Fine-Tuned Features. ArXiv abs/2412.01555 (2024). <https://api.semanticscholar.org/CorpusID:27443731>

[28] Deepjyoti Roy and Mala Dutta. 2022. A systematic review and research perspective on recommender systems. *Journal of Big Data* 9, 1 (May 2022). doi:10.1186/s40537-022-00592-5

[29] Erich Schubert, Arthur Zimek, and Hans-Peter Kriegel. 2015. *Fast and Scalable Outlier Detection with Approximate Nearest Neighbor Ensembles*. Springer International Publishing, 19–36. doi:10.1007/978-3-319-18123-3_2

[30] Harsha Vardhan Simhadri, George Williams, Martin Aumüller, Matthijs Douze, Artem Babenko, Dmitry Baranichuk, Qi Chen, Lucas Hosseini, Ravishankar Krishnaswamy, Gopal Srinivasa, Suhas Jayaram Subramanya, and Jingdong Wang. 2022. Results of the NeurIPS'21 Challenge on Billion-Scale Approximate Nearest Neighbor Search. arXiv:2205.03763 [cs.LG] <https://arxiv.org/abs/2205.03763>

[31] Aditi Singh, Suhas Jayaram Subramanya, Ravishankar Krishnaswamy, and Harsha Vardhan Simhadri. 2021. FreshDiskANN: A Fast and Accurate Graph-Based ANN Index for Streaming Similarity Search. doi:10.48550/ARXIV.2105.09613

[32] Pradeep Kumar Singh, Pijush Kanti Dutta Pramanik, Avick Kumar Dey, and Prasenjit Choudhury. 2021. Recommender systems: an overview, research trends, and future directions. *International Journal of Business and Systems Research* 15, 1 (2021), 14. doi:10.1504/ijbsr.2021.111753

[33] Sivic and Zisserman. 2003. Video Google: a text retrieval approach to object matching in videos. In *Proceedings Ninth IEEE International Conference on Computer Vision*. IEEE, 1470–1477 vol.2. doi:10.1109/iccv.2003.1238663

[34] Yiping Sun, Yang Shi, and Jiaolong Du. 2024. A Real-Time Adaptive Multi-Stream GPU System For Online Approximate Nearest Neighborhood Search. In *Proceedings of the 33rd ACM International Conference on Information and Knowledge Management (CIKM '24)*. ACM, 4906–4913. doi:10.1145/3627673.3680054

[35] Karthik Venkatasubba, Saim Khan, Somesh Singh, Harsha Vardhan Simhadri, and Jyothi Vedurada. 2025. BANG: Billion-Scale Approximate Nearest Neighbour Search Using a Single GPU. *IEEE Transactions on Big Data* 11, 6 (Dec. 2025), 3142–3157. doi:10.1109/tbdata.2025.3581085

[36] Hui Wang, Wan-Lei Zhao, Xiangxiang Zeng, and Jianye Yang. 2021. Fast k-NN Graph Construction by GPU based NN-Descent. In *Proceedings of the 30th ACM International Conference on Information & Knowledge Management (CIKM '21)*. ACM, 1929–1938. doi:10.1145/3459637.3482344

[37] Shijie Wang, Wenqi Fan, Yue Feng, Lin Shanru, Xinyu Ma, Shuaiqiang Wang, and Dawei Yin. 2025. Knowledge Graph Retrieval-Augmented Generation for LLM-based Recommendation. In *Proceedings of the 63rd Annual Meeting of the Association for Computational Linguistics (Volume 1: Long Papers)*. Association for Computational Linguistics, 27152–27168. doi:10.18653/v1/2025.acl-long.1317

[38] Tevin Wang, Jingyuan He, and Chenyan Xiong. 2024. RAGViz: Diagnose and Visualize Retrieval-Augmented Generation. In *Proceedings of the 2024 Conference on Empirical Methods in Natural Language Processing: System Demonstrations*. Association for Computational Linguistics, 320–327. doi:10.18653/v1/2024.emnlp-demo.33

[39] Samuel Williams, Andrew Waterman, and David Patterson. 2009. Roofline: an insightful visual performance model for multicore architectures. *Commun. ACM* 52, 4 (April 2009), 65–76. doi:10.1145/1498765.1498785

[40] Yan Xia, Kaiming He, Fang Wen, and Jian Sun. 2013. Joint Inverted Indexing. In *2013 IEEE International Conference on Computer Vision*. IEEE, 3416–3423. doi:10.1109/iccv.2013.424

- [41] Yuanhang Yu, Dong Wen, Ying Zhang, Lu Qin, Wenjie Zhang, and Xuemin Lin. 2022. GPU-accelerated Proximity Graph Approximate Nearest Neighbor Search and Construction. In *2022 IEEE 38th International Conference on Data Engineering (ICDE)*. IEEE, 552–564. doi:10.1109/icde53745.2022.00046
- [42] Weijie Zhao, Shulong Tan, and Ping Li. 2020. SONG: Approximate Nearest Neighbor Search on GPU. In *2020 IEEE 36th International Conference on Data Engineering (ICDE)*. IEEE. doi:10.1109/icde48307.2020.00094
- [43] Yifan Zhu, Ruiyao Ma, Baihua Zheng, Xiangyu Ke, Lu Chen, and Yunjun Gao. 2024. GTS: GPU-based Tree Index for Fast Similarity Search. *Proceedings of the ACM on Management of Data* 2, 3 (May 2024), 1–27. doi:10.1145/3654945